A Schrödinger-Poisson Solver for Modeling Carbon Nanotube FETs

D.L. John†, L.C. Castro†, P.J.S. Pereira, and D.L. Pulfrey

Department of Electrical and Computer Engineering
The University of British Columbia
Vancouver, BC V6T 1Z4, Canada

ABSTRACT

We present details of a coupled Schrödinger-Poisson solver for modeling quantum transport effects in carbon nanotube field-effect transistors. The Poisson solution is effected using a two-dimensional finite difference algorithm in a coaxial structure with azimuthal symmetry. The Schrödinger solution is implemented by the scattering matrix method, and the resultant, spatially unbounded wavefunctions, defined on the nanotube surface, are normalized to the flux computed by the Landauer formula. The solver illustrates the need for detailed modeling of the nanotube due to the impact of interference effects and evanescent modes on the carrier profiles. Non-equilibrium carrier distributions are presented for particular cases.

Keywords: carbon nanotubes, modeling, nanoelectronics, transistors, quantum transport

1 INTRODUCTION

Carbon nanotubes [1] are attracting great interest for their use in nanoscale electronic devices. Recent modeling efforts of carbon nanotube field-effect transistors (CNFETs) have been successful in examining the subthreshold behaviour of these devices through a simple solution to Laplace's equation [2], [3], while the above-threshold behaviour has been modeled using bulk device concepts [4], [5]. Accurate CNFET modeling requires a self-consistent solution of the charge and local electrostatic potential. In order to properly treat such quantum phenomena as tunneling and resonance, the charge is computed via Schrödinger's equation. Owing to the presence of metal-semiconductor interfaces, we also account for the penetration of evanescent wavefunctions from the metal into the energy gap of the nanotube.

We deal specifically with the coaxial geometry of the CNFET shown in Fig. 1. The device consists of a semiconducting carbon nanotube surrounded by insulating material (relative permittivity ϵ_{ins}) and a cylindrical, wrap-around gate contact. The source and drain contacts terminate the ends of the device. The device dimensions of note are the gate radius, R_g, the nanotube radius, R_t, the insulator thickness $t_{\text{ins}} = R_g - R_t$, and the device length, L_t.

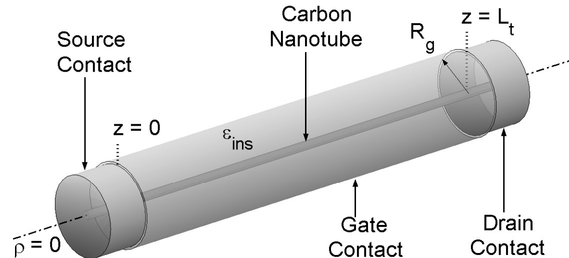

Figure 1: Coaxial CNFET model geometry.

In this closed, metallic cylinder system, Poisson's equation, restricted to just two dimensions by azimuthal symmetry, is

$$\frac{\partial^2 V}{\partial \rho^2} + \frac{1}{\rho}\frac{\partial V}{\partial \rho} + \frac{\partial^2 V}{\partial z^2} = -\frac{Q}{\epsilon}\,, \tag{1}$$

where $V(\rho, z)$ is the potential within the outer cylinder, and Q is the charge density. It must be noted that, although the solution of Eq. (1) encompasses the entire volume of the device, we are primarily concerned with the longitudinal potential profile along the surface of the tube, hereafter labeled $V_{CS}(z) \equiv V(R_t, z)$, since knowledge of this potential is required for carrier transport calculations.

We treat the nanotube as a quasi-one-dimensional conductor, and the linear carrier density is then computed via the time-independent Schrödinger equation given by

$$\frac{\partial^2 \Psi}{\partial z^2} = -\frac{2m}{\hbar^2}\left(E - U\right)\Psi\,, \tag{2}$$

where $\Psi(z, E)$ is the wavefunction of a carrier with total energy E and effective mass m, traveling in a region with local effective potential $U(z)$. While Q may include sources such as trapped charge within the dielectric, we neglect any charge other than that of electrons and holes on the nanotube.

2 SOLUTION METHOD

We require a solution to Eq. (1) with $Q = Q(V)$. Convergence for this non-linear system is achieved with

†These authors contributed equally to this work.

the Picard iterative scheme, whereby iteration $k+1$ is given by

$$V_{k+1} = V_k - \alpha \mathcal{L}^{-1} r_k \,,$$

$$r_k = \mathcal{L} V_k + Q(V_k) \,,$$

where r_k is the residual of the k-th iteration, $0 < \alpha \leq 1$ is a damping parameter, and $\mathcal{L}$ represents the linear, differential operator allowing Eq. (1) to be written as $\mathcal{L}V = -Q$.

2.1 Potential

The boundary conditions for V are given by

$$V(R_g, z) = V_{GS} - \phi_G/q \,, \tag{3}$$

$$V(\rho, 0) = -\phi_S/q \,, \tag{4}$$

$$V(\rho, L_t) = V_{DS} - \phi_D/q \,, \tag{5}$$

$$\frac{\partial V}{\partial \rho}(0, z) = 0 \,, \tag{6}$$

where $\phi_{G,S,D}$ represent the work functions of the gate-, source-, and drain-metallizations, respectively, and V_{GS} and V_{DS} are the gate- and drain-source voltages. Due to the discontinuity in ϵ across the nanotube surface, we must also apply the usual matching condition

$$\epsilon_{\rm ins} \frac{\partial V}{\partial \rho}\bigg|_{R_t^+} - \epsilon_t \frac{\partial V}{\partial \rho}\bigg|_{R_t^-} = -\frac{q(p-n)}{2\pi R_t} \,,$$

where p and n are the one-dimensional hole and electron carrier densities.

The solution to Eq. (1) was obtained via the finite difference technique, implemented by discretizing the spatial domain and using central differencing to generate a linear system of equations, for some known Q, and subject to the boundary conditions specified by Eqs. (3)–(6). Finite differencing was chosen over an FFT-Green's function approach due to its flexibility in modeling more complex structures. The singularity at $\rho = 0$ was addressed by applying l'Hôpital's Rule to the offending term, yielding

$$\frac{1}{\rho}\frac{\partial V}{\partial \rho} \simeq \frac{\partial^2 V}{\partial \rho^2} \,.$$

The amount of energy band bending in the vacuum level, along the length of the nanotube, is given by $E_{vac}(z) = -qV_{CS}(z)$, since we assume that the local electrostatic potential rigidly shifts the nanotube band structure. The potential energies seen by electrons and holes in the nanotube are

$$U_e(z) = E_{vac}(z) - \chi_{CN} \,, \tag{7}$$

$$U_h(z) = -U_e(z) + E_g \,, \tag{8}$$

where E_g and χ_{CN} are, respectively, the nanotube bandgap and electron affinity.

2.2 Charge

Having established a solution for the potential and its relation to the energy band structure, we now determine the carrier concentration. In our system, the charge density is given by

$$Q = \frac{q(p-n)}{2\pi}\frac{\delta(\rho - R_t)}{\rho} \,,$$

where $\delta(\cdot)/\rho$ is the Dirac delta function in cylindrical coordinates, and $n(z)$ and $p(z)$ are computed via Eq. (2), where the nanotube effective mass is obtained from the tight-binding approximation of the band structure, and is the same for both electrons and holes due to symmetry [1]. Only the first, doubly-degenerate band is included in the calculations presented herein. The potential energy, U, for each carrier type is specified by Eqs. (7)–(8), given a potential profile $V_{CS}(z)$.

We solve Eq. (2) using the scattering-matrix method in which a numerical solution is propagated by cascading 2×2 matrices [6]. We find that the use of piecewise constant potentials (plane-wave solutions) are preferable to piecewise linear potentials (Airy function solutions) due to the considerable reduction of simulation time without an appreciable increase in the error. Matching of the wavefunction and its derivative on the boundary between intervals n and $n+1$, assuming a constant effective mass, is performed via the usual relations

$$\Psi_n = \Psi_{n+1} \,,$$

$$\frac{\partial \Psi_n}{\partial z} = \frac{\partial \Psi_{n+1}}{\partial z} \,.$$

In order to completely specify the wavefunction, we require two boundary conditions. In the contacts, the wavefunction at a given energy is of the form

$$\Psi = \begin{cases} A{\rm e}^{{\rm i}k_S z} + B{\rm e}^{-{\rm i}k_S z} & , \quad z < 0 \,, \\ C{\rm e}^{{\rm i}k_D z} + D{\rm e}^{-{\rm i}k_D z} & , \quad z > L_t \,, \end{cases}$$

where k_S and k_D are the wavevectors in the source and drain contacts, respectively, and A, B, C, and D are constants. As an example, noting that an analogous calculation may be performed for the drain by exchange of variables, we now illustrate source injection. For this case, $D = 0$ for all energies. In addition, we expect that the Landauer equation [7] will hold for the flux, and must be equal to the probability current. For the transmitted wave, this yields

$$\frac{2q}{\pi\hbar} f_S T = \frac{q\hbar}{m} k_D |C|^2 \,, \tag{9}$$

where the pre-factor of 2 accounts for the aforementioned band degeneracy, f_S is the Fermi-Dirac carrier distribution in the source, and T is the transmission probability specified by

$$T = \frac{k_D |C|^2}{k_S |A|^2} \,.$$

Simple manipulation yields the normalization condition

$$|A|^2 = \frac{2m}{\pi\hbar^2}\frac{f_S}{k_S}\,. \tag{10}$$

At any given energy, multiplication of the unnormalized wavefunction by a constant satisfies Eq. (10).

Including source and drain injection components, the normalized wavefunctions yield the total carrier densities in the system,

$$n(z) = \int_{\mathcal{E}_e}^{\infty} \left(|\Psi_{e,S}|^2 + |\Psi_{e,D}|^2 \right) \mathrm{d}E\,,$$

$$p(z) = \int_{\mathcal{E}_h}^{\infty} \left(|\Psi_{h,S}|^2 + |\Psi_{h,D}|^2 \right) \mathrm{d}E\,,$$

where $\mathcal{E}_{e,h}$ is taken to be the bottom of the band, for either electrons or holes, in the appropriate metallic contact, and corresponds to the bottom of the band in the metal. In practice, the integrals are performed using adaptive Romberg integration, where repeated Richardson extrapolations are performed until a predefined tolerance is reached [8]. We find that an adaptive integration method is a necessity for convergence, in order to properly capture Ψ, which is typically highly-peaked in energy for propagating modes. Alternatively, one could employ a very fine discretization in energy, however the Romberg method allows for the mesh size to change based on the requirements of the integrand, and results in a much improved simulation time.

3 RESULTS

We now present results for a CNFET with a (16, 0) nanotube ($R_t \approx 0.63$ nm; $E_g \approx 0.62$ eV), $L_t = 20$ nm, $t_{\text{ins}} = 2.5$ nm, and $\epsilon_{\text{ins}} = 25$. All work functions are taken to be 4.5 eV unless otherwise noted, and $\chi_{CN} = 4.2$ eV. The nanotube is presumed to have a free-space relative permittivity $\epsilon_t = 1$ [9], and $\mathcal{E}$ was taken to be 5.5 eV below the metal Fermi level, as a rough estimate [10].

In equilibrium, *i.e.*, for $V_{DS} = 0$, we obtain reasonable agreement for the carrier concentrations away from the contacts with that computed using equilibrium statistics [2]. Out of equilibrium, however, interference effects influence the carrier distributions throughout the device. Fig. 2 shows the carrier distributions for $V_{GS} = 0.5$ V as a function of position and V_{DS}, and Fig. 3 shows the corresponding conduction band edges for $V_{DS} = 0$ and 0.4 V.

Under a positive gate bias, the band bending results in an increase in the electron concentration throughout the device as more propagating modes are allowed in the channel. As V_{DS} is increased, this concentration is considerably reduced in the mid-length region. Evanescent modes dominate the carrier concentrations near the end contacts, thus impacting on the local potential. Due to

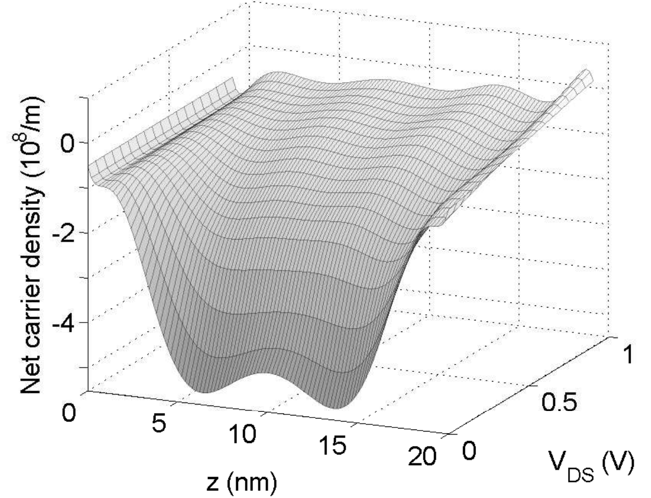

Figure 2: Net carrier density, $p(z) - n(z)$, for the model device as a function of position and V_{DS}.

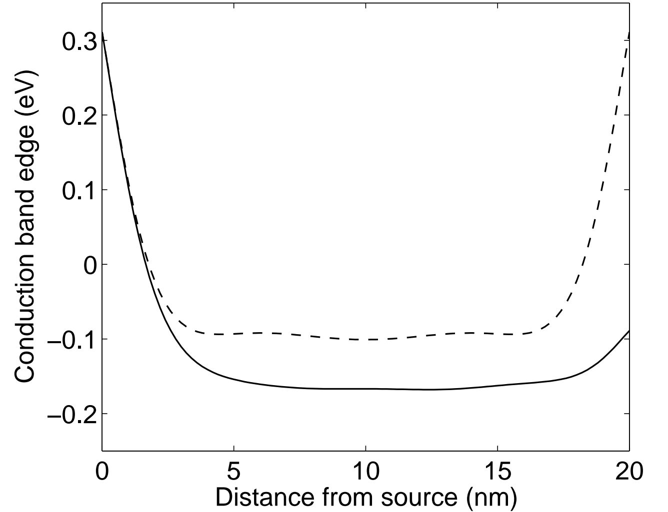

Figure 3: Conduction band edges for the model device with $V_{GS} = 0.5$ V, and $V_{DS} = 0$ (dashed) and 0.4 V (solid). Energies are with respect to the source Fermi level.

the exponential dependence of the transmission probability on the barrier shapes, the flux is significantly modified if these modes are neglected.

We note, also, that it is important to allow for the full inclusion of quantum mechanical reflection for the thermionic component of the flux. Often, carriers above the barrier are assumed to have a transmission probability near unity. However, this approximation does not hold in general, as Fig. 4 shows, wherein the significant reflection is due to $\mathcal{E}$ being much lower than the conduction band edge. The effect is most important for devices where the metal-nanotube work function differ-

ence yields a negative barrier, shown in Fig. 4(a). Here, a classical treatment would considerably overestimate the Landauer flux, a function of T, for energies in the vicinity of the Fermi level.

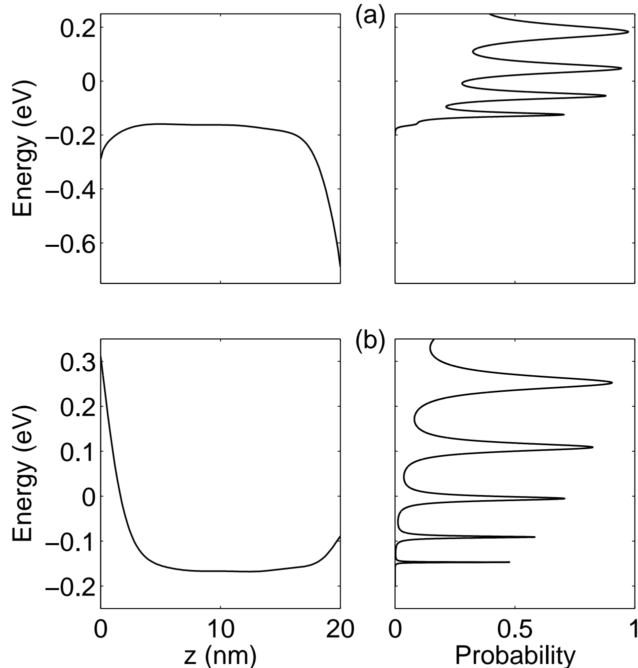

Figure 4: Conduction band edges and transmission probabilities for electrons at $V_{GS} = 0.5\,\mathrm{V}$ and $V_{DS} = 0.4\,\mathrm{V}$: (a) $\phi_S = \phi_D = 3.9\,\mathrm{eV}$ and (b) $\phi_S = \phi_D = 4.5\,\mathrm{eV}$. Energies are with respect to the source Fermi level.

Finally, the present Schrödinger-Poisson method allows for explicit calculation of the carrier distribution functions, as shown in Fig. 5. The result is in marked contrast to a previous self-consistent model [5] that utilized quasi-equilibrium distribution functions to calculate the non-equilibrium carrier concentrations. Moreover, while the model provided in Ref. [4] yields more appropriate non-equilibrium carrier distributions, it is not equipped to account for the resonant peaks illustrated here.

4 CONCLUSIONS

From this work on the modeling of CNFETs with a coupled Schrödinger-Poisson solver, we conclude that:

1. equilibrium statistics are not adequate in describing the carrier distributions in energy;

2. consideration of the evanescent modes is crucial for the accurate simulation of devices where transport is dominated by tunneling through the interfacial barriers;

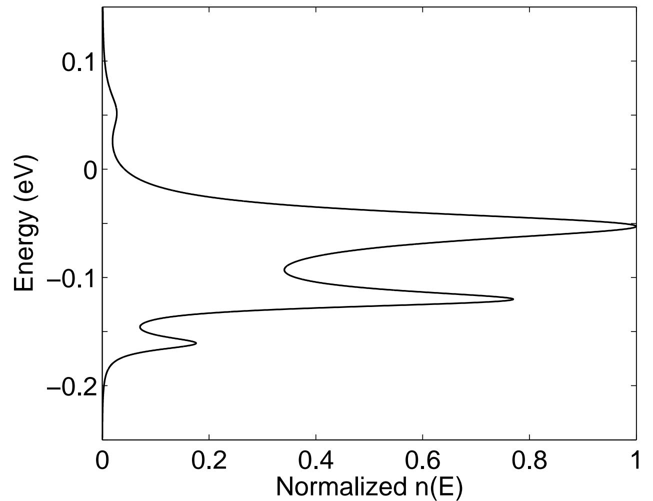

Figure 5: Source-originated electron concentration at $L_t/2$, normalized to its maximum value. $V_{GS} = 0.5\,\mathrm{V}$, $V_{DS} = 0.4\,\mathrm{V}$, and $\phi_S = \phi_D = 3.9\,\mathrm{eV}$. Energies are with respect to the source Fermi level.

3. for devices dominated by thermionic emission, a full solution of Schrödinger's equation is still required in order to account for significant reflection above the barriers.

REFERENCES

[1] R. Saito, T. Takeya, T. Kimura, G. Dresselhaus, and M.S. Dresselhaus, Phys. Rev. B, 57, 4145, 1998.

[2] D.L. John, L.C. Castro, J.P. Clifford, and D.L. Pulfrey, IEEE Trans. Nanotechnol., 2, 175, 2003.

[3] S. Heinze, M. Radosavljević, J. Tersoff, and Ph. Avouris, Phys. Rev. B, 68, 235418, 2003.

[4] L.C. Castro, D.L. John, and D.L. Pulfrey, Proc. IEEE COMMAD, 303–306, 2002.

[5] J.P. Clifford, D.L. John, and D.L. Pulfrey, IEEE Trans. Nanotechnol., 2, 181, 2003.

[6] D.Y.K. Ko and J.C. Inkson, Phys. Rev. B, 38, 9945, 1988.

[7] D.K. Ferry and S.M. Goodnick, Transport in Nanostructures, Cambridge University Press, New York, 1997.

[8] L.W. Johnson and R.D. Riess, Numerical Analysis, Addision-Wesley, Don Mills, Ontario, 1977.

[9] F. Léonard and J. Tersoff, Appl. Phys. Lett., 81, 4835, 2002.

[10] N.W. Ashcroft and N.D. Mermin, Solid State Physics, Harcourt College Publishers, New York, 1st edn., 1976.